Electrochimica Acta 397 (2021) 139277

Contents lists available at ScienceDirect

Electrochimica Acta

journal homepage: www.elsevier.com/locate/electacta

Deviations from linearity in impedance spectroscopy measurements confirmed by Kramers-Kronig analysis

G. Barbero[a,b], F. Batalioto[c], A.M. Figueiredo Neto[c], I. Lelidis[d,*]

[a] Dipartimento di Scienza Applicata del Politecnico di Torino, Corso Duca degli Abruzzi 24, Torino, 10129, Italia
[b] National Research Nuclear University MEPhI (Moscow Engineering Physics Institute), Kashirskoye shosse 31, Moscow, 115409, Russian Federation
[c] Instituto de Física, Universidade de São Paulo, Rua do Matão 1371, São Paulo, 05508-090, SP, Brazil
[d] Faculty of Physics, National and Kapodistrian University of Athens, Panepistimiopolis, Zografos, Athens, 157 84, Greece

ARTICLE INFO

Article history:
Received 6 June 2021
Revised 14 September 2021
Accepted 15 September 2021
Available online 21 September 2021

Keywords:
Electrochemical impedance spectroscopy
Kramers - Kronig analysis
Linearity assessment method
Frequency dependance of linearity

ABSTRACT

We investigate the electric response of a kerosene cell containing magnetic nanoparticles. The cell is submitted to an external potential difference and its impedance is measured for increasing values of the potential amplitude. The analysis of the experimental data by means of the Kramers-Kronig relations indicates an unexpected deviation from the linear behaviour situated close to the frequency identifying the minimum of the cell's reactance modulus. We show that this departure from linearity could be related to the imaginary part of the ions' bulk density when its variation cannot be considered as a small quantity. The analysis is performed in the one-type mobile ions approximation of the Poisson-Nernst-Planck model assuming Ohmic boundary conditions on the electrodes. Fitting the data using linear models gives poor results any time the Kramers-Kronig analysis shows deviations from linearity.

1. Introduction

The analysis of the electric response of an electrolytic cell to an external excitation in the low frequency region is strongly dependent on the presence of the ions dissolved in the electrolytic solution. The impedance spectroscopy technique allows to investigate the response of the cell by changing the frequency of the applied voltage. It allows the experimental measurement of the impedance of the cell from which the real, $\mathcal{R}$, and imaginary, $\mathcal{X}$, parts, in the series representation, are derived. The quantity $\mathcal{R}$ is related to the dissipative, while $\mathcal{X}$ to the reactive, phenomena taking place into the cell. Of course, the concept of impedance is meaningful only if the system is linear, and hence for an excitation at circular frequency ω, the current in the circuit has a component only at ω.

An analysis of the impedance of the cell, in the linear limit, based on the equations of continuity for the ions and on the equation of Poisson relating the actual potential to the bulk densities of ions, has been proposed long ago by Macdonald [1,2], and is known as the Poisson-Nernst-Planck (PNP) model which has been recently reconsidered and generalized by several authors [3–12]. In this case, the Kramers-Kronig relations (KKR) valid for linear systems, are obviously verified. For a stable and causal system, a deviation from KKR is an indication that the system does not behave in a linear manner[13]. The analysis of an electrolytic cell indicates that the conditions of linearity are always verified in the high frequency region [14]. In this context, high frequency means frequency larger than the Debye circular frequency defined as the ratio between the diffusion coefficient of the ions in the liquid and the squared Debye length. Debye length represents the thickness of the surface layer in which the ions are confined in the dc case [15]. In the low frequency region, in particular in the dc limit, the response of the cell depends on the properties of the electrodes[16], and the validity of the linear approximation critically depends on the amplitude of the applied voltage [14]. On the contrary, in the high frequency region the response of the cell is independent of the electrodes, and the system behaves as a linear dielectric medium with losses. If the system exhibits non-linearity then any conclusion from the analysis of the experimental data may be misleading. Therefore a great effort has been performed towards the validation of the system's linearity using the KKR [17–19].

In recent measurements performed on cells of kerosene containing magnetic particle, we have observed unexpected deviations from the linear behaviour localized on a frequency range close to the frequency identifying the minimum of the modulus of the reactance of the cell [20]. In the present paper, our goal is to show that these deviations are related to the partial violation of the linearity condition, and to determine the frequency range in which these deviations may appear.

* corresponding author.:.
E-mail address: ilelidis@phys.uoa.gr (I. Lelidis).

https://doi.org/10.1016/j.electacta.2021.139277
0013-4686/

The paper is organized as follows. In Section 2, we briefly recall the linear PNP model for only one type of mobile ions. In particular, we introduce the linearity condition and give the solution of the model for an electrolytic cell with ohmic boundary conditions. In Section 3, we discuss the validity of the linear approximation and show that deviations from linearity are expected in a specific frequency range that can be predicted. Section 4 describes briefly the experimental set-up and materials. In Section 5, we test the linearity of the data sets by fitting them. In Section 6, we demonstrate the non-linearity of the data sets using the Kramers-Kronig transformations. Finally, Section 7 is devoted to conclusions.

2. Linear approximation

We limit our analysis to a cell of the type considered in [20], relevant to kerosene with magnetic particles. In this case, a good description of the response of the cell, in the shape of a slab of thickness d and surface area S, can be achieved in the one-type mobile ions approximation. In the system under consideration the presence of ions in the solution is attributed to a residual concentration of sodium oleate from the synthesis procedure. The solution is globally neutral, but in the presence of an external electric field it becomes locally charged, since mobile ions move under the effect of the electric field. In this framework, the magnetic grains are assumed immobile, and just the ions of one sign dissolved in the kerosene contribute to the response of the cell. This assumption repose on the experimental evidence that the diffusion coefficient, for Stokes' formula [15], depends on the geometrical dimensions, and the free ions are very small with respect to magnetic grains. Note that when more than one group of ions are present, then the superposition principle is not valid in general [21]. We indicate by ε the dielectric constant of the pure kerosene, n_0 the bulk density of ions, in thermodynamical equilibrium, n_p the bulk density of ions when the cell is submitted to an external voltage, by q the electric charge of the ions, and by D_p their diffusion coefficient in kerosene. The problem is one dimensional. The cartesian reference frame used in the analysis has the z-axis perpendicular to the electrodes, placed at $z = \pm d/2$. The equation of continuity for the mobile ions and the equation of Poisson are [20]

$$\frac{\partial n_p}{\partial t} = D_p \frac{\partial}{\partial z}\left(\frac{\partial n_p}{\partial z} + \frac{q n_p}{k_B T}\frac{\partial V}{\partial z}\right), \tag{1}$$

$$\frac{\partial^2 V}{\partial z^2} = -\frac{q}{\varepsilon}(n_p - n_0). \tag{2}$$

The first term in the r.h.s. of Equation (1) describes the diffusion of particles. The second one represents the drift current in presence of an electric field. This equation is valid in the Einstein approximation, where the mobility of the ions, μ_p, and their diffusion coefficient, D_p, are related by the equation $\mu_p/D_p = k_B T/q$, and the generation-recombination phenomenon can be neglected. This assumption, in our case of small ionic density, is reasonable [22]. The other fundamental equation of the model, (2), relates the actual electric potential in the cell with the ionic charge density. We define the dimensionless quantities

$$u_p = \frac{n_p - n_0}{n_0}, \quad \text{and} \quad u_v = \frac{qV}{k_B T}, \tag{3}$$

and rewrite (1,2) as

$$\frac{\partial u_p}{\partial t} = D_p \frac{\partial}{\partial z}\left(\frac{\partial u_p}{\partial z} + (1+u_p)\frac{\partial u_v}{\partial z}\right) \tag{4}$$

$$\frac{\partial^2 u_v}{\partial z^2} = -\frac{1}{\Lambda^2} u_p, \tag{5}$$

where $\Lambda = \sqrt{\varepsilon V_{\rm th}/(n_0 q)}$ is the Debye length, and $V_{\rm th} = k_B T/q$ the thermal voltage, of the order of 25 mV at room temperature.

In the linear approximation approach, in (4) it is assumed that

$$1 + u_p \sim 1, \quad \text{i.e.} \quad u_p \ll 1. \tag{6}$$

In this framework, indicating by u_p^0 and u_v^0 the linear approximation of u_p and u_v, the partial differential equations by means of which the system under consideration is described are

$$\frac{\partial u_p^0}{\partial t} = D_p \frac{\partial}{\partial z}\left(\frac{\partial u_p^0}{\partial z} + \frac{\partial u_v^0}{\partial z}\right) \tag{7}$$

$$\frac{\partial^2 u_v^0}{\partial z^2} = -\frac{1}{\Lambda^2} u_p^0, \tag{8}$$

For an harmonic external excitation, u_p^0 and u_v^0 can be written as

$$u_p^0(z,t) = \phi_p(z)\,\exp(i\omega t), \quad u_v^0(z,t) = \phi_v(z)\,\exp(i\omega t). \tag{9}$$

where $\omega = 2\pi f$ is the circular frequency and f the frequency of the applied signal. Substituting (9) into (7,8) we get

$$i\frac{\omega}{D_p}\phi_p(z) = \phi_p''(z) + \phi_v''(z), \tag{10}$$

$$\phi_v''(z) = -\frac{1}{\Lambda^2}\phi_p(z). \tag{11}$$

We assume that the electrode are not blocking, and the charge exchange on them is well described by the Ohmic model [16]. Therefore the ordinary differential equations (10,11) have to be solved with the following boundary conditions

$$\phi_p' + B\phi_v' = 0, \quad \phi_v = \pm u_0/2, \quad \text{for} \quad z = \pm d/2. \tag{12}$$

where the Ohmic properties of the electrodes are contained in the parameter B defined by means of an intrinsic surface conductivity $\kappa_c = n_0 D/V_{\rm th}$, and of a characteristic conductivity of the electrode κ, such that $B = 1 - \kappa/\kappa_c$. The case of blocking electrodes is recovered putting $\kappa = 0$ [21]. u_0 is the reduced amplitude of the potential difference applied between the electrodes. From (10,11) we obtain

$$\phi_p''(z) - \beta^2\phi(z) = 0, \tag{13}$$

where

$$\beta = \frac{1}{\Lambda}\sqrt{1 - i\Omega}, \tag{14}$$

with $\Omega = \omega/\omega_D$ and $\omega_D = D_p/\Lambda^2$ is the Debye's frequency [21]. As discussed elsewhere [20], the spatial components $\phi_p(z)$ and $\phi_v(z)$ are

$$\phi_p(z) = C_p\,\sinh(\beta z), \tag{15}$$

$$\phi_v(z) = -\frac{1}{\beta^2\Lambda^2}C_p\,\sinh(\beta z) + C_v z, \tag{16}$$

where the integration constants C_p and C_v are determined by (12). They are found to be

$$C_p = -\frac{\beta^2\Lambda^2 B}{2B + \beta d(-B + \beta^2\Lambda^2)\coth(\beta d/2)}\frac{u_0}{\sinh(\beta d/2)},$$

$$C_v = \beta\frac{-B + \beta^2\Lambda^2}{\beta d(-B + \beta^2\Lambda^2) + 2B\tanh(\beta d/2)}\,u_0.$$

In this way the linear problem is solved. Of course, the linear solution is meaningful only if condition (6) is verified in the entire frequency range. Note that the solution (15) is a complex quantity. Therefore at the electrodes, where the potential amplitude is a real

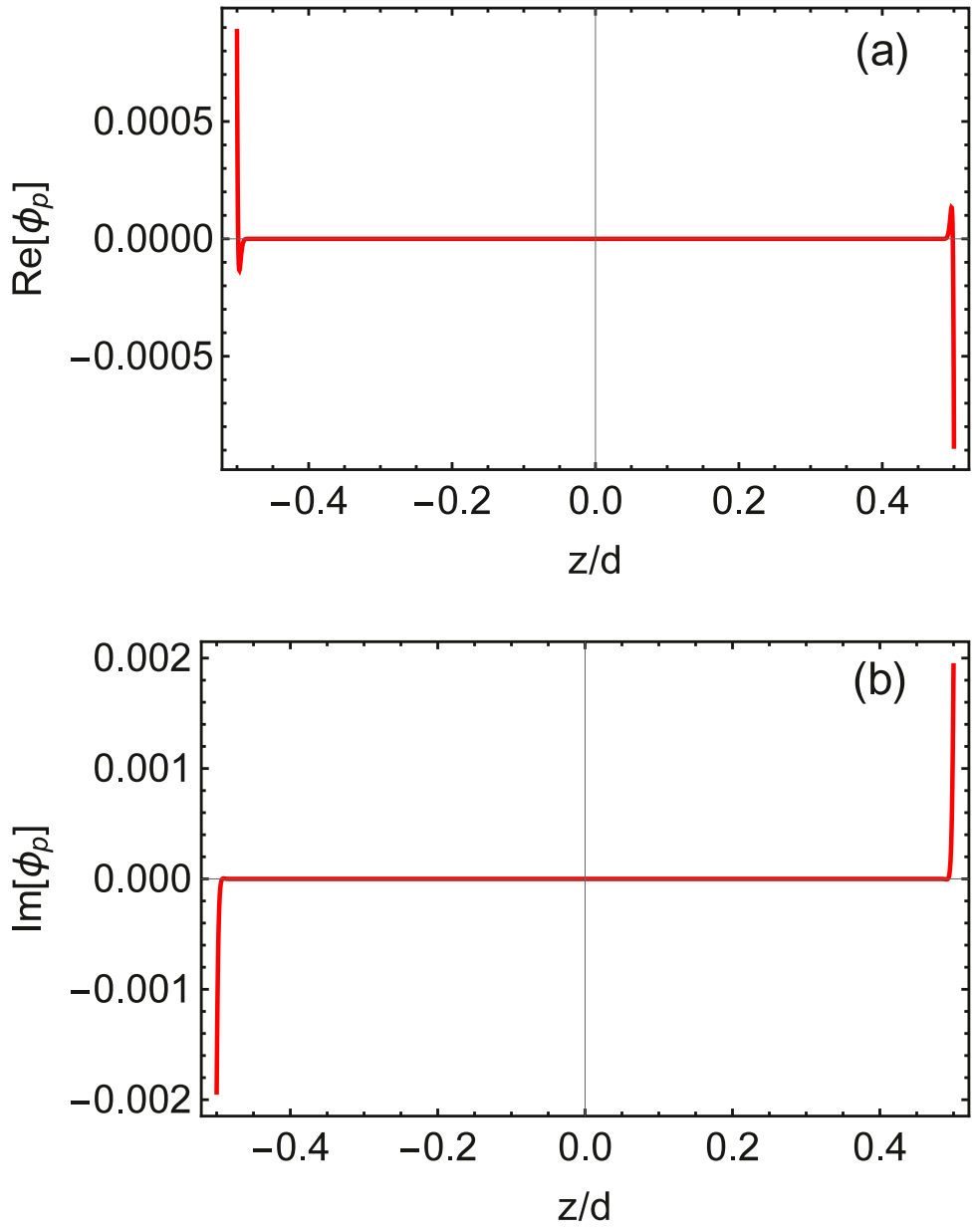

Fig. 1. Profiles of the real, (a), and imaginary, (b), parts of the bulk density of ions across the cell. They show a strong position dependence close to the electrodes, in a surface layer of thickness of a few Debye lengths. $f = 1$ kHz, $u_0 = 1$.

quantity, the ionic density is not in phase with the applied potential.

In the linear limit, substituting the expression of C_p into (15) we get $\phi_p(z) \propto \sinh(\beta z)/\sinh(\beta d/2)$, where, as it follows from (14), for $\Omega < 1$, $\beta \sim 1/\Lambda$. As it will be discussed later, $d \gg \Lambda$, and hence $|\phi_p|$ tends to zero in the bulk over a distance of a few Λ. In other words, the ionic charge is localized in two surface layers whose thickness is of the order of a few Λ.

3. Validity of the linear approximation

As stressed at the end of the preceding section, the linear approximation implies the validity of the inequality (6) in the frequency range in which the derived formulae are applied. Using the expression of u_p^0, one can investigate the validity of the conditions (6).

As it follows from (15) and (16), $\phi_p(z)$ is a complex function. Its real, $R_p(z) = \mathrm{Re}[\phi_p(z)]$, and imaginary, $I_p = \mathrm{Im}[\phi_p(z)]$, components are shown in Fig. 1 on the range $-1/2 \le z/d \le 1/2$. For the numerical calculation we assume $q = 1.6 \times 10^{-19}$ A s, $\varepsilon = 2 \times \varepsilon_0$, $n_0 = 1.48 \times 10^{21}$ m^{-3}, $D_p = 1.23 \times 10^{-11}$ m^2/s, and the ohmic parameter $\kappa = 9.8 \times 10^8$ m^{-1}s^{-1}V^{-1}, as determined in [20,23]. Using these values one calculates the Debye length $\Lambda = 4.73 \times 10^{-8}$ m. The geometrical parameters of the cell are $d = 24\,\mu$m$>> \Lambda$ and $S = 10^{-4}$ m^2. Fig. 2 is a zoom of Fig. 1 in the range $(d/2) + 5\Lambda \le z \le d/2$, for $f = 1$ kHz and $u_0 = 1$. As it is evident from these figures, $|R_p|$ and $|I_p|$ are odd functions, and reach their maximum value on the electrodes. This is valid for all frequencies of the applied signal.

For this reason, since we are interested in the limit of validity of the linear approximation, in the following we limit our considerations to

$$\phi_p(d/2) = -\frac{\beta^2\Lambda^2 B}{2B + \beta d(-B + \beta^2\Lambda^2)\coth(\beta d/2)}\,u_0. \tag{17}$$

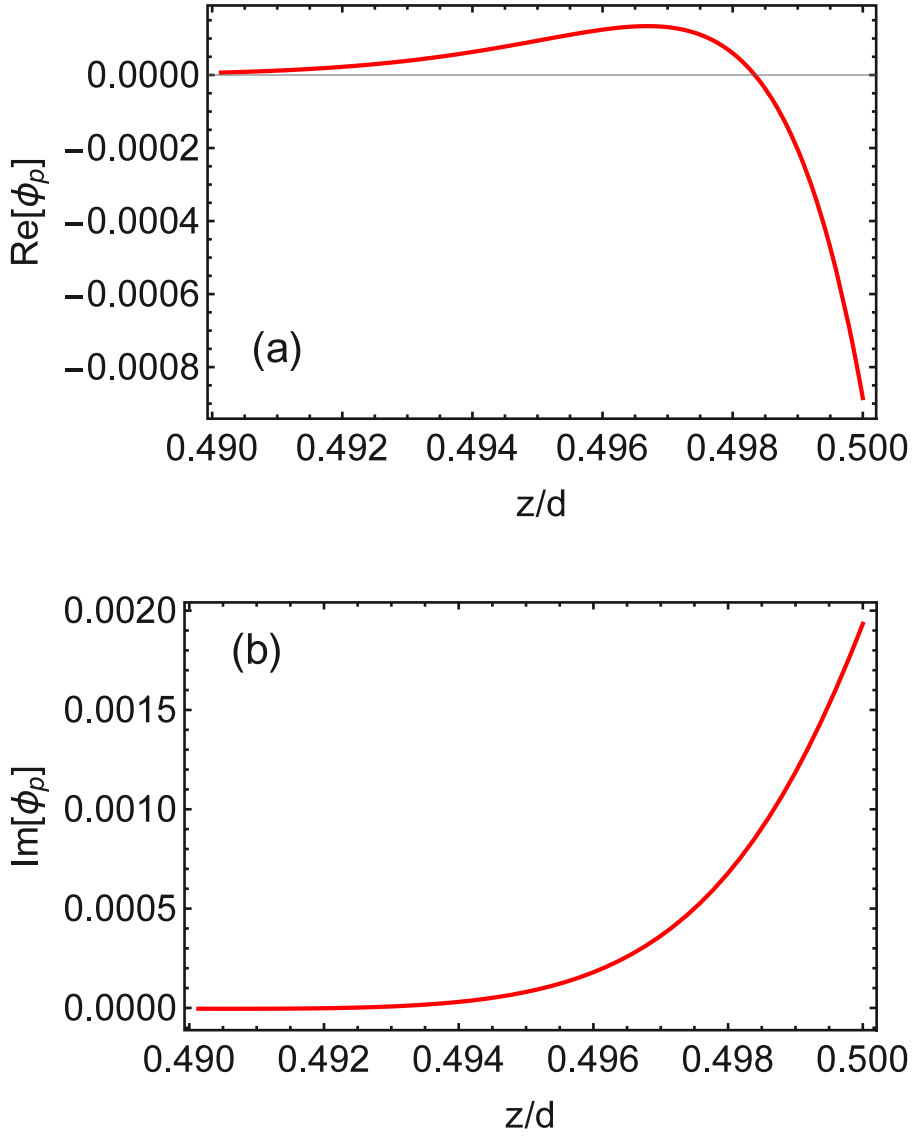

Fig. 2. Profiles of the real, (a), and imaginary, (b), parts of the bulk density of ions, in a surface layer of thickness 5Λ. The functions $|R_p|$ and $|I_p|$ reach their maximum values on the electrodes.

The validity of the linear analysis based on the validity of condition (6) implies

$$R_p \ll 1, \quad \text{and} \quad I_p \text{ very small.} \tag{18}$$

In the cases of interest, $|\beta d/2| \gg 1$, and hence $\coth(\beta d/2) \sim 1$. Taking into account the definition of β, (17) can be rewritten as

$$\phi_p(d/2) = -\frac{\beta^2 \Lambda^2 B}{2B + \beta d(-B + \beta^2 \Lambda^2)}\, u_0. \tag{19}$$

In Fig. 3 we show the frequency dependence of the real, (a), and imaginary, (b), parts of the bulk density of ions on the electrodes (at $z = d/2$) for three values of the reduced applied voltage.

From (17) it follows

$$\lim_{f\to 0} R_p = -\frac{u_0}{2}, \quad \& \quad \lim_{f\to 0} I_p = 0, \tag{20}$$

$$\lim_{f\to \infty} R_p = \lim_{f\to \infty} I_p = 0. \tag{21}$$

Consequently, in the dc limit the main limitation is related to R_p, whereas, in the high frequency region the linear approximation is always valid [14]. In the dc limit the ionic density variation is in phase with the external electric field. On the contrary, in the high frequency region, the ionic contribution to the response of the cell, to the external electric field, is negligible. Consequently the system behaves as an insulating medium. For frequency lower, but of the order of the Debye frequency, I_p is large, and could limit the validity of the linear approximation. In fact, according to conditions (18), R_p has to be compared with 1, whereas I_p has to be small. Hence we have not a concrete upper limit to which compare I_p. Therefore only a numerical analysis allows to investigate the validity of the linear approximation.

We have analyzed, numerically, the maximum of I_p versus Λ. According to our results the frequency at which I_p becomes maximum is

$$\omega^* = 2\frac{\Lambda}{d}\,\omega_D, \quad \& \quad I_p(\omega^*) = \frac{u_0}{4}. \tag{22}$$

The calculated value $u_0/4$ is an upper limit since ϕ_p goes rapidly to zero in the bulk (see Fig. 1). In Fig. 4 is shown the reduced frequency ω^*/ω_D versus Λ/d and the approximation (22). From the analysis reported above, it follows that possible deviations from

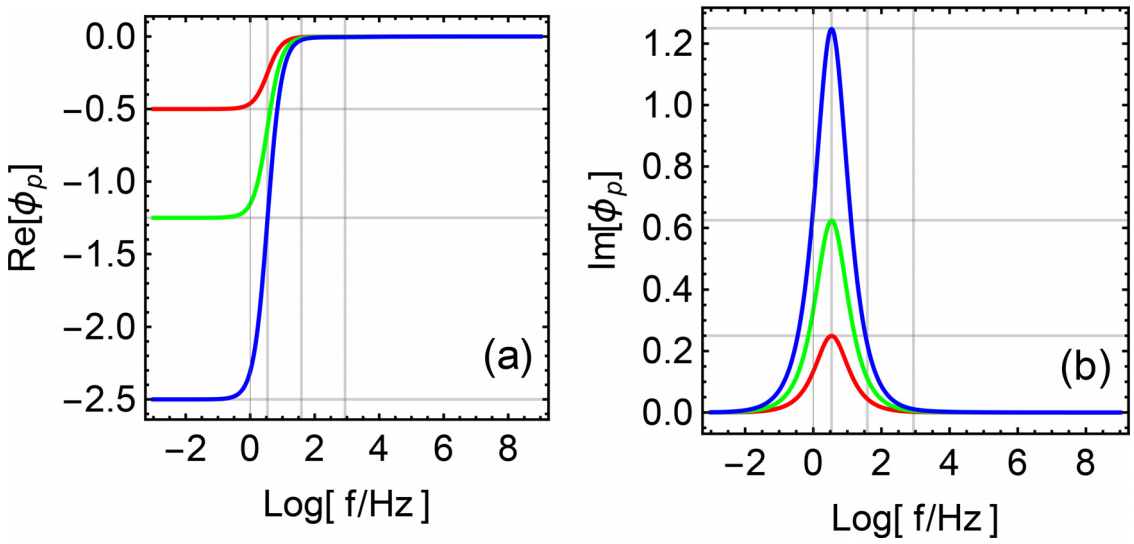

Fig. 3. Frequency, f dependencies of the real, (a), and imaginary, (b), part of the bulk density of ions on the electrodes. The real part is a monotonic decreasing function of the frequency, whereas, the imaginary part presents a well defined maximum at a frequency lower that the frequency of Debye. The curves are drawn for $u_0 = 1$, red, $u_0 = 2.5$, green, and $u_0 = 5$, blue. In the dc limit R_p tends to $-u_0/2$, and I_p to zero. In the high frequency region both R_p and I_p tend to zero, and the linear approximation is always valid. (For interpretation of the references to colour in this figure legend, the reader is referred to the web version of this article.)

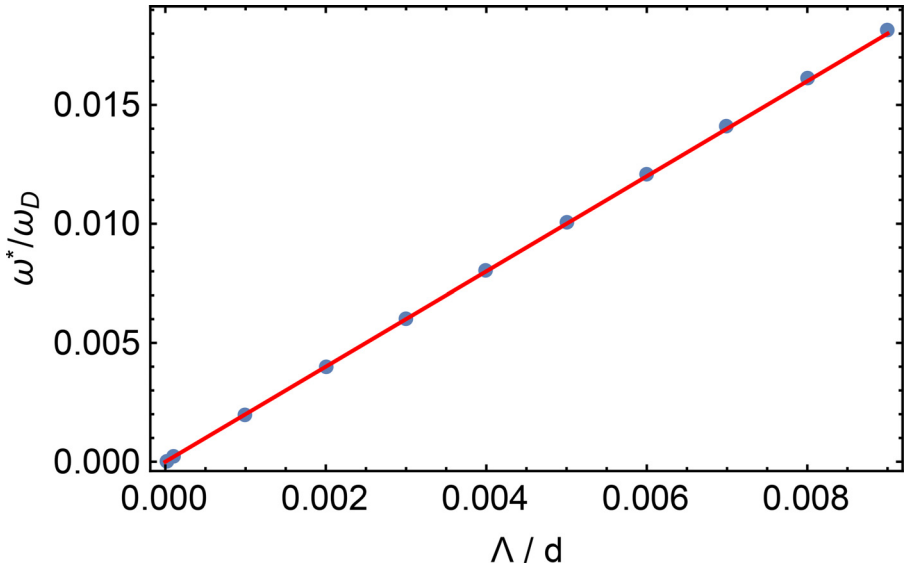

Fig. 4. Reduced frequency ω^*/ω_D of the I_p maximum versus Λ/d. Points are numerically determined. Line is calculated from the model, expression $\omega^* = 2(\Lambda/d)\omega_D$.

the linear behavior could appear when I_p is not a small quantity. This condition could be violated near to the frequency ω^*.

4. Experimental set up and material

The experimental data refer to a cell of ferrofluid of thickness $d = 24\,\mu$m, described in [23], submitted to an external sinusoidal voltage of amplitude V_0 ranging from 25 mV to 3V. The used ferrofluid consisted of about $10^{22}\,m^{-3}$ (1%vol) spherical nanoparticles of typical mean size $\sim$ 18nm suspended in kerosene. The sample was inserted between two disk-like electrodes made of brass of area $S = 10.2\,cm^2$. The impedance was then measured by means of a Solartron 1260A Impedance/Gain-Phase analyzer with a 12962A sample holder from 10mHz to 1.6MHz. As discussed in [23], the electrodes in brass are well described by the Ohmic model. We note that measurements similar to those discussed in the present paper relevant to electrodes in brass, have been performed also with electrodes in gold, titanium and surgical steel [20]. The reported spectra were only weakly dependent on the nature of the electrodes.

5. Limit of validity of the linear model: Fitting

The fundamental equations of the linear PNP-model are, obviously, linear partial equations [2,24–26]. Hence, they describe the response of an ideal linear medium. Therefore the best fitting is expected to describe poorly any non-linear data set.

Hereupon, our analysis is described in terms of resistance and reactance, since we measure experimentally the impedance of the cell. If one relates the surface charge density with the electric field close to the electrodes using Coulomb theorem then the current is deduced and subsequently the impedance may be calculated [7]. In the case of blocking electrodes, according to PNP-model, $\mathcal{R}$ presents a large plateau that ends at the Debye frequency ω_D. For $\omega \gg \omega_D$, $\mathcal{R} \propto 1/\omega^2$. In the same framework, $|\mathcal{X}|$ diverges in the dc limit as $1/\omega$. Increasing ω, it presents a minimum at

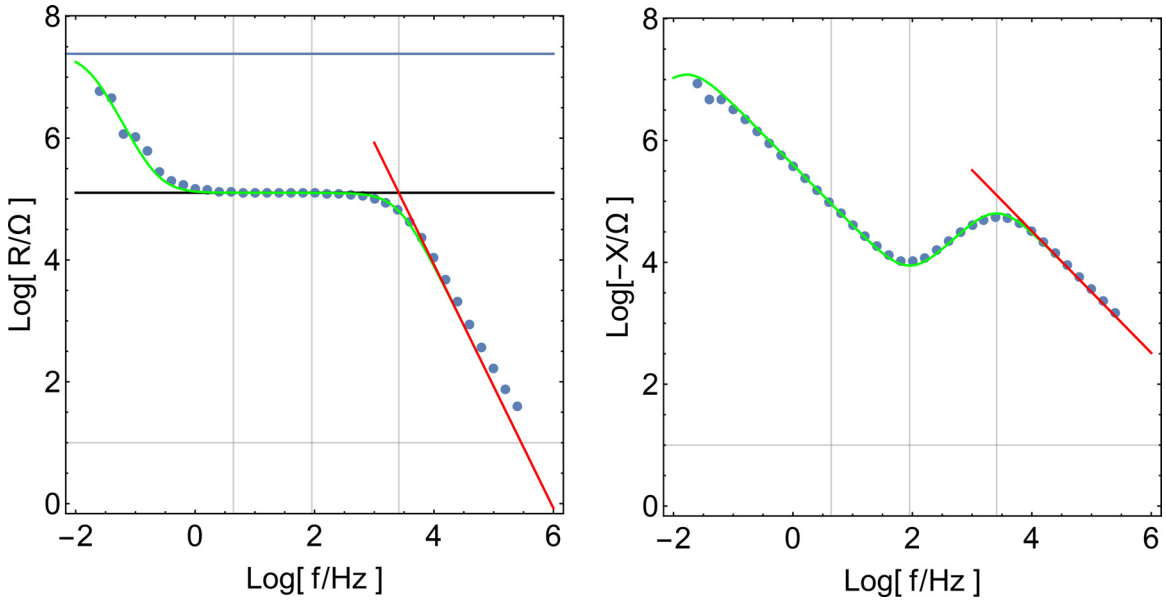

Fig. 5. Resistence, $\mathcal{R}$, and reactance, $\mathcal{X}$, vs frequency f. Thickness of the cell $d = 24\ \mu$m. Harmonic signal amplitude $V_0 = 25$ mV. Experimental data, points; PNP-model fitting, green line. The red line at high frequencies gives the resistance/reactance of the cell as calculated by (28). (For interpretation of the references to colour in this figure legend, the reader is referred to the web version of this article.)

$\omega_m = \sqrt{2\Lambda/d}\ \omega_D$, and a maximum at $\omega = \omega_D$. For $\omega \gg \omega_D$, $|\mathcal{X}| \propto 1/\omega$, [27]. In the dc limit, the divergence of $|\mathcal{X}|$ is due, according to PNP model, to the formation of a surface capacitance, related to the confinement of the ions in a surface layer of thickness of the order of Λ, $C_s = \varepsilon S/\Lambda$. On the contrary, in the opposite limit of high frequency, $|\mathcal{X}| \propto 1/\omega$ indicates that in this region of the spectrum, the ions do not participate any longer to the electric conduction, and the system behave as a perfect insulator, whose capacitance is simply $C_b = \varepsilon S/d$.

In the low frequency region, the predictions of the PNP-model reported above, are valid only if the electrodes can be considered as blocking, i.e., only if there is not any conduction current in the dc limit. If this condition is not satisfied, in the dc limit $\mathcal{R}$ presents a new plateau, whose value depends on the electrode properties, i.e., on the ohmic parameter κ introduced above. In the same limit, $|\mathcal{X}|$ tends to zero with ω, indicating that the predominant character of the cell is related to the surface conductivity of the electrodes, allowing a charge exchange between the bulk and the external circuit [27]. The fit quality of the experimental data obtained by the PNP-model with Ohmic boundary condition [28], is rather good in the limit of small values of the applied potential difference amplitude V_0. As discussed in [20], in the one-mobile ion limit with Ohmic boundary conditions, the impedance $\mathcal{Z} = \mathcal{R} + i\mathcal{X}$ of the sample is given by

$$\mathcal{Z} = \frac{\beta d(-B + \beta^2\lambda^2) + 2B\tanh(\beta d/2)}{\beta^3 \varepsilon S D(-b + \beta^2\Lambda^2)}, \tag{23}$$

that in our case, where $d \gg \Lambda$, is well approximated by

$$\mathcal{Z} = \frac{\beta d(-B + \beta^2\Lambda^2) + 2B}{\beta^3 \varepsilon S D(-b + \beta^2\Lambda^2)}. \tag{24}$$

From (24), in the limit $\omega \to 0$, the impedance tends to

$$\mathcal{R}_0 = \lim_{\omega\to 0} \mathcal{Z}(\omega) = \frac{\Lambda^2 d}{\varepsilon D S} + 2\,\frac{\Lambda^3 B}{D\varepsilon S(1-S)}. \tag{25}$$

The first addendum is independent of the electrode properties. Hence it can be identified with the bulk resistance, $\mathcal{R}_b$, in the dc limit, of a cell limited by blocking electrodes. From the definition of the Debye frequency, ω_D, this contribution can be recast in the form

$$\mathcal{R}_b = \frac{1}{\omega_D \varepsilon}\ \frac{d}{S}. \tag{26}$$

As to the second addendum in (25), it is related to the Ohmic properties of the electrodes. Taking into account the definition of B, and that according to our experimental data $\kappa \ll \kappa_c$, this contribution is

$$2\,\mathcal{R}_e = 2\,\frac{\Lambda}{\kappa q S}. \tag{27}$$

The expression of $\mathcal{R}_e$ indicates that in the dc limit the contribution of the electrodes is localized in a surface layer of thickness of the order of Λ, and it is due to the surface electric conductivity $\sigma_e = q\kappa$. In the dc limit, the electric impedance of the cell reduces to a resistance of the electrodes, in series with the resistance of the bulk:

$$\lim_{\omega\to 0} \mathcal{Z}_b = \mathcal{R}_b + 2\,\mathcal{R}_e.$$

In the high frequency region ($\omega \gg \omega_D$), from (2) we get

$$\lim_{\omega\to\infty} \mathcal{Z}(\omega) = -i\frac{1}{\omega\varepsilon}\ \frac{d}{S} + \mathcal{R}_b\left(\frac{\omega_D}{\omega}\right)^2. \tag{28}$$

It follows that, in the high frequency region, the cell behaves as a real condenser of capacitance $\mathcal{C}_b = \varepsilon S/d$, and resistance $(\omega_D/\omega)^2\,\mathcal{R}_b$. In Figs. 5, 6, 7, 8, we show the real and imaginary parts of the cell impedance for a few values of the external excitation amplitude V_0. The best fits have been obtained for $N_0 = 8.3 \times 10^{21}$ m^{-3}, $\varepsilon = 1.3 \times \varepsilon_0$, $D = 0.35 \times 10^{-11}$ m^2/s, and $\kappa = 0.75 \times 10^7$ 1/(m s V), which are of the same order of magnitude with the values obtained for a similar ferrofluid investigated in [20]. As it is evident from the reported figures, the quality of the fit decreases with increasing V_0, although in the high frequency region, it remains good enough for all considered V_0 values.

On the $\mathcal{R} = \mathcal{R}(\omega)$ spectra the upper horizontal line indicates the dc resistance of the cell, $\mathcal{R}_0 = 2\mathcal{R}_e + \mathcal{R}_b$, whereas the lower horizontal line corresponds to the bulk resistance of the cell $\mathcal{R}_b$, related to a cell limited by blocking electrodes. The straight line (in red) corresponds to the resistance of the cell in the high frequency region, given by (28). The vertical lines, from left to right,

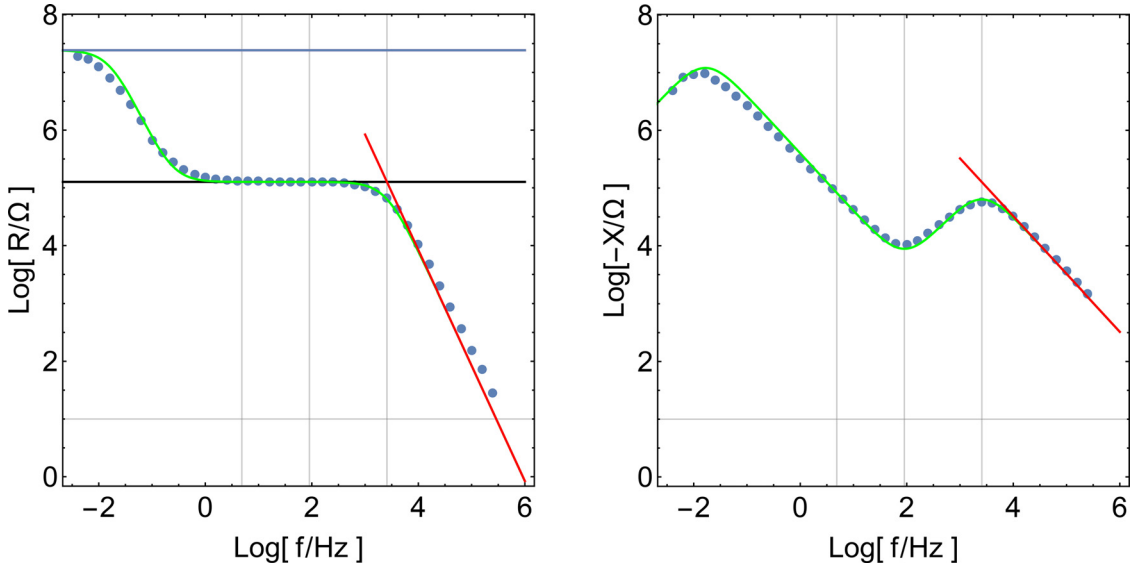

Fig. 6. Real, $\mathcal{R}$, and imaginary part, $\mathcal{X}$, of the electric impedance vs frequency f. The cell, of thickness $d = 24\ \mu$m, is submitted to a harmonic signal of amplitude $V_0 = 115$ mV. Symbols as in Fig. 5. Note that the deviations between the experimental $\mathcal{X}$-data and the theoretical prediction first appear at f^*.

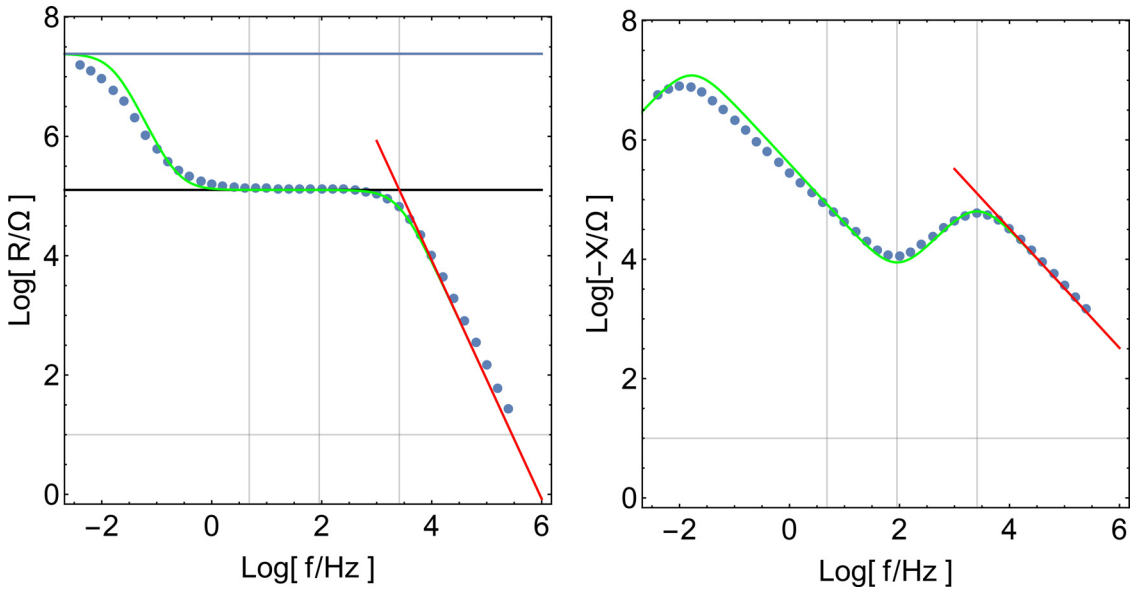

Fig. 7. Spectra of the real, $\mathcal{R}$, and imaginary, $\mathcal{X}$, part of the electric impedance vs frequency f. Thickness of the cell $d = 24\ \mu$m. The cell is submitted to a harmonic signal of amplitude $V_0 = 200$ mV. Symbols as in Fig. 5. Note that the deviation between the experimental data relevant to the reactance and the theoretical prediction takes place at the frequency f^*.

identify the frequency ω^* at which the imaginary part of the bulk density of ions presents a maximum, and the circular frequencies, $\omega_m = \sqrt{2\lambda/d}\ \omega_D$, and ω_D for which $|\mathcal{X}|$ has a minimum and a maximum, respectively. The continuous curve is the best fit of the experimental data, shown by solid points, obtained by means of the PNP linear model, in the one-type mobile ions approximation.

On the $\mathcal{X} = \mathcal{X}(\omega)$ spectra, the straight line, in the high frequency region is the reactance of the cell, related to the capacitance $\mathcal{C}_b = \varepsilon S/d$, and the vertical lines correspond to ω^*, ω_m and ω_D respectively from the left. The green continuous lines are the best fit of the experimental data (blue points). As it is shown in Figs. 6, 7, 8, for $V_0 = 115$ mV, $V_0 = 200$ mV and $V_0 = 345$ mV, the deviations of the fitting from the experimental data with decreasing frequency first appear in the neighborhood of ω^*, in agreement with the discussion reported above.

6. Limit of validity of the linear model: Kramers-Kronig transformations

In the previous section we demonstrated that the best fit procedure, using the linear PNP model, is unable to fit correctly some data set. Of course one could object that either our fitting procedure simply doesn't succeed to find the correct parameter set, or the PNP model simply fails to describe the data for reasons that do not imply a non-linearity issue. In order to prove that our data cannot be described from any linear model, hereupon we use the Kramers-Kronig transformation to test the non-linearity issue.

For systems that satisfy the conditions of linearity, stability and causality one expects that the resistance (real, $\mathcal{R}$, part), and the reactance (imaginary, $\mathcal{X}$, part) of the impedance verify the Kramers-Kronig relations (KKR) [29–33]. For the system under considera-

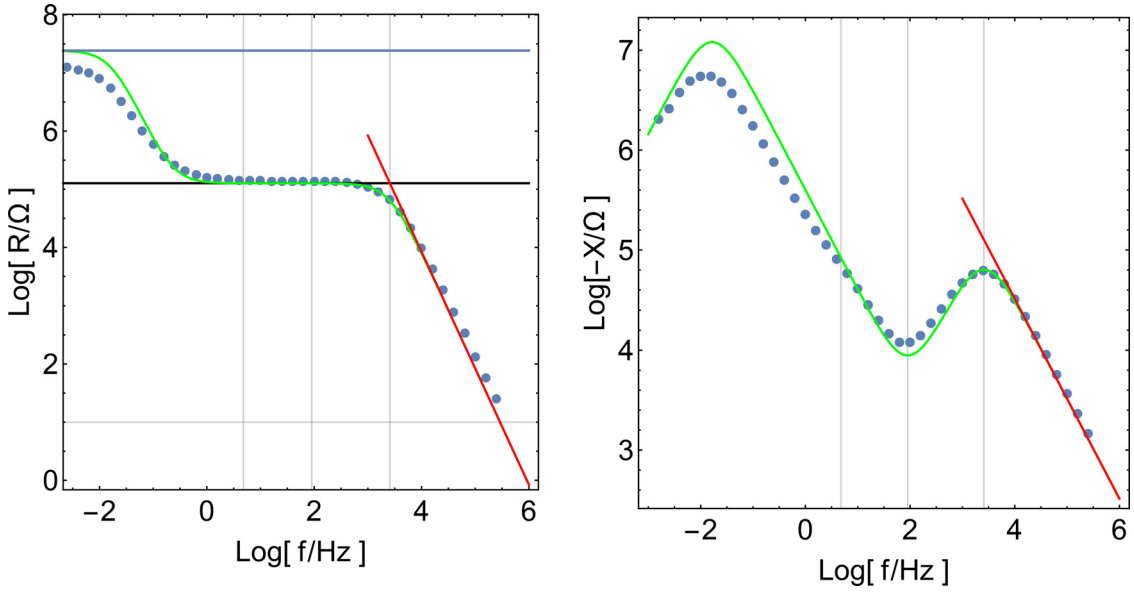

Fig. 8. Real, $\mathcal{R}$, and imaginary, $\mathcal{X}$, part of the electric impedance vs frequency f. Cell of thickness $d = 24\ \mu$m. Harmonic signal of amplitude $V_0 = 345$ mV. Symbols as in Fig. 5. The experimental data of reactance deviate from the theoretical prediction at the frequency f^*.

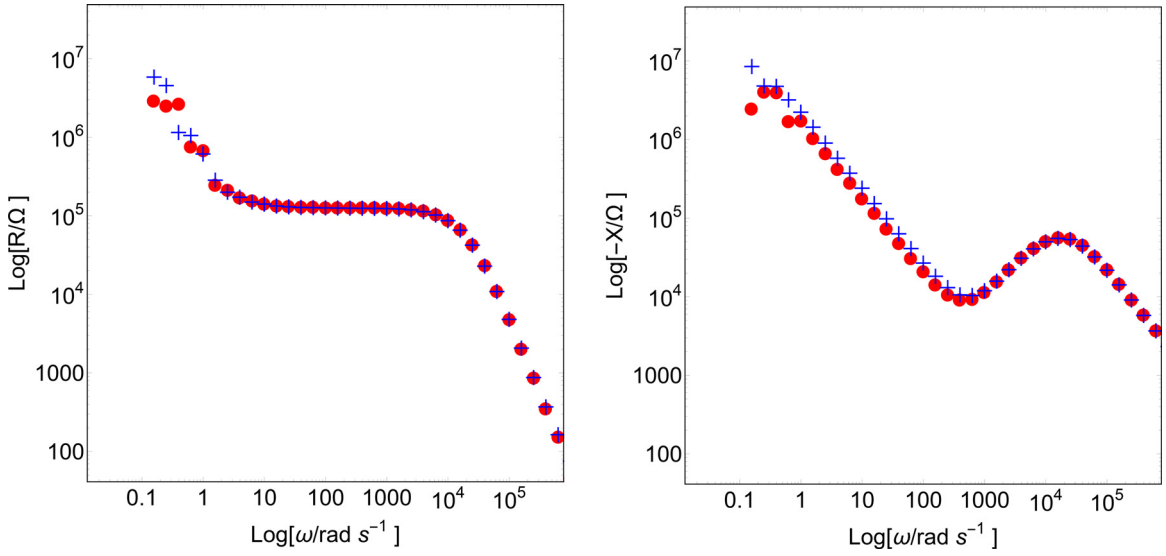

Fig. 9. Resistence $\mathcal{R}$, and reactance $\mathcal{X}$ vs frequency ω. Applied potential amplitude $V_0 = 25$mV. Experimental data are marked with blue crosses. Calculated data derived by Kramers-Kronig relations are marked with red points. The overall agreement between experimental and calculated data points is satisfactory. Note that in the low frequency range data are scattered because of thermal noise. (For interpretation of the references to colour in this figure legend, the reader is referred to the web version of this article.)

tion, the KKR are

$$\mathcal{R}(\omega) = -\frac{2}{\pi}\,\mathcal{P}\int_0^\infty \frac{\omega'\mathcal{X}(\omega')}{\omega'^2-\omega^2}\,d\omega' \tag{29}$$

$$\mathcal{X}(\omega) = -\frac{2\omega}{\pi}\,\mathcal{P}\int_0^\infty \frac{\mathcal{R}(\omega')}{\omega'^2-\omega^2}\,d\omega' \tag{30}$$

where $\mathcal{P}$ means the Cauchy principal part of the integral, on the real axis. Equations (29) and (30) coincide with equations (22.58), and (22.57) reported in Chapter 22 of [29], respectively.

Our point is that the KKR can be used to test the linearity condition for a response function in a causal and stable system. Therefore, we use KKR to produce the real from the imaginary part of the sample's impedance and vice versa [34]. The results are compared with the measured ones. Any systematic discrepancy between the measured function and the calculated one could signal deviation from linearity. In Figs. 9, 10, 11,12, we compare the experimental spectra, blue crosses, of $\mathcal{R}$ and $\mathcal{X}$ vs the circular frequency ω for various values of applied potential, V_0, at the sample's electrodes with the corresponding ones derived by the KKR, red points. Fig. 9 shows the experimental and the KK-calculated points for the thermal voltage ($V_0 = 25$mV). The agreement is questionable in the low frequency range. Nevertheless the observed deviations at low frequency result from the thermal noise because the applied voltage is apparently too low. This can be inferred from the experimental data which are scattered at the low frequencies. Fig. 10 shows the results for $V_0 = 115$mV. The agreement is reasonable good in the entire ω-range. Increasing more the applied voltage to $V_0 = 345$mV, Fig. 11, one observes some deviations of the KK-calculated points in respect to the experimen-

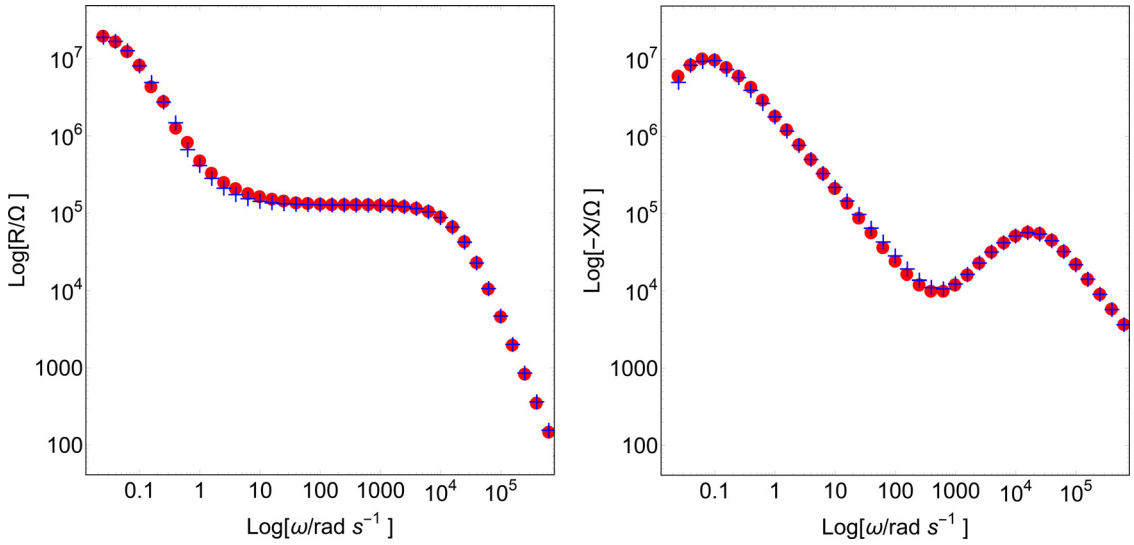

Fig. 10. Resistence $\mathcal{R}$, and reactance $\mathcal{X}$ vs frequency ω. Applied potential amplitude $V_0 = 115$mV. Symbols as in Fig. 9. The overall agreement between experimental and calculated data points is satisfactory.

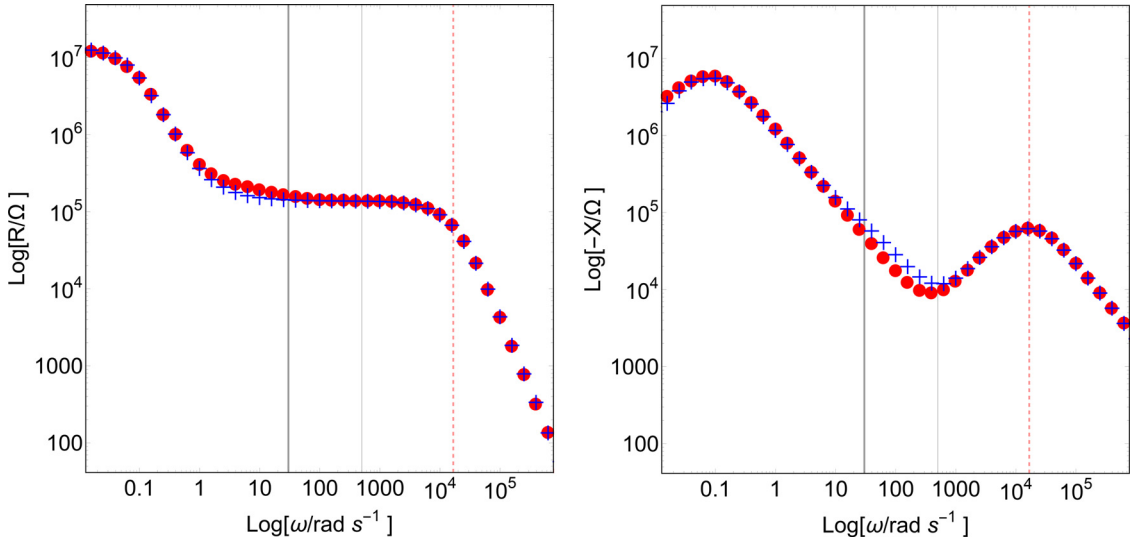

Fig. 11. Resistence $\mathcal{R}$, and reactance $\mathcal{X}$ vs frequency ω. Applied potential amplitude $V_0 = 345$mV. Symbols as in Fig. 9. Deviations between experimental and KK-calculated data points are observed in the intermediate frequency range for the imaginary part. The red-dashed line indicates the position of the Debye frequency. The thin gray line indicates the minimum of $|\mathcal{X}|$. The thick gray line indicates the present model's prediction for ω^* around which deviations from linearity are expected. (For interpretation of the references to colour in this figure legend, the reader is referred to the web version of this article.)

tal data especially for the imaginary part. These deviations are located in the middle frequency range while the accordance at lower and higher frequencies is fair. Deviations appear roughly about the minimum of $|\mathcal{X}(\omega)|$ and spread up towards lower frequencies. In Figs. 11–12, are shown the Debye frequency by a red-dashed line, the frequency, ω_m, where the minimum of $|\mathcal{X}(\omega)|$ occurs, thin-blue line, and the frequency ω^* around which deviations from linearity should appear in accordance to our model. Finally at 3V, Fig. 12, the deviations become much stronger and are clearly observed in both $\mathcal{R}(\omega)$, and $\mathcal{X}(\omega)$. For the calculation of the ratio Λ/d that is requested in order to obtain ω^* from (22), we use the relation $\omega_{\min} = \sqrt{\Lambda/d}\,\omega_D$ valid for ohmic electrodes [27] while $\omega_{\min}$ and ω_D are evaluated from the experimental data minimum and high frequency maximum of $|\mathcal{X}(\omega)|$. Finally, ω^* is given from the relation $\omega^* = 2\omega_{\min}^2/\omega_D$. As one can deduce by simple inspection of Figs. 11 & 12, ω^* is located in the ω-range where departure from linearity is observed.

7. Conclusions

We used the Kramers-Kronig relations as a test to investigate the linearity of a physical system. For this aim, we measured the complex impedance function of a sample for increasing values of the applied voltage at its electrodes. We show that for high enough amplitude of the applied voltage a deviation from linear behavior appears in the imaginary part of the system's impedance. The deviation starts at frequencies around the minimum of the absolute value of the reactance and propagates towards lower frequencies. Our results are described by considering the limit of validity of the linear version of PNP-model requiring that the relative variation of the bulk density of ions has to be small with respect to 1. In the case of harmonic excitation this relative variation is represented by a complex quantity, and the condition of small relative variation implies a condition on its real and imaginary parts. From the analysis on the condition relevant to the real part we show that it has to be small with respect to 1. On the contrary, for what concerns

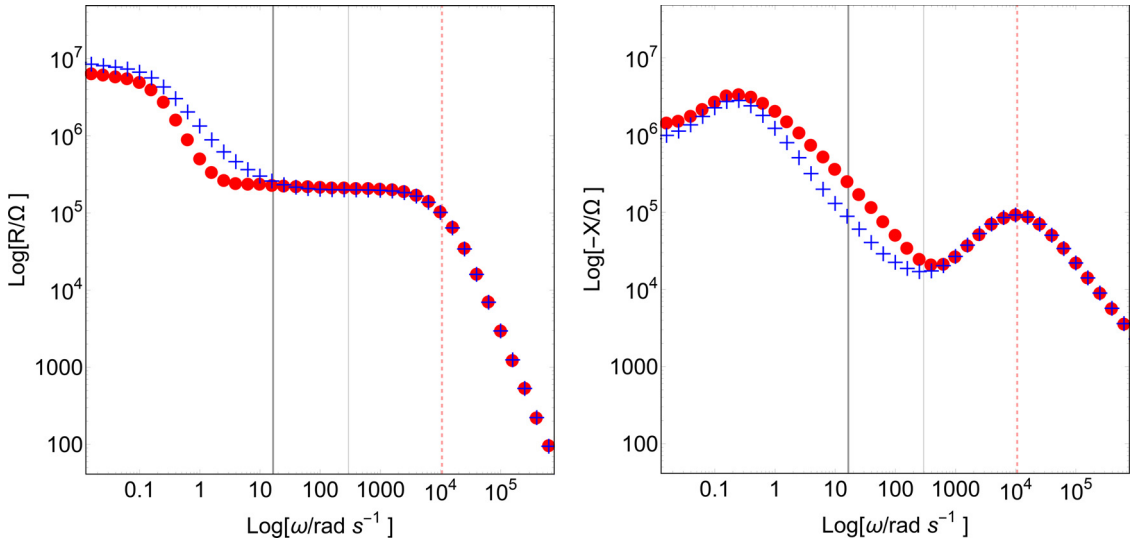

Fig. 12. Resistence $\mathcal{R}$, and reactance $\mathcal{X}$ vs frequency ω. Applied potential amplitude $V_0 = 3$V. Symbols as in Fig. 9. Large deviations between experimental and KK-calculated data points are observed for both real and imaginary parts. Vertical lines as in Fig. 11.

the imaginary part, it has to be small in absolute, and hence possible deviations from the validity of the linear version are connected with this not very well defined inequality. The presented analysis has been performed analyzing the analytical solution, deduced assuming the validity of the linear version of PNP-model, and investigating the frequency range where the assumption of validity are verified. From the analysis of the frequency dependence of the imaginary part of the relative density variation, we have derived the frequency around which deviations in what concerns the validity of the model are expected. The theoretical predictions, about deviations from linearity with increasing applied potential, are in reasonable agreement with the observed deviations when analyzing the experimental data both by using the best fit approach, and by means of Kramers-Kronig relations.

Disclosure of conflicts of interest

The authors declare that they have no known competing financial interests or personal relationships that could have appeared to influence the work reported in this paper.

Declaration of Competing Interest

The authors declare no conflict of interest.

Credit authorship contribution statement

G. Barbero: Conceptualization, Methodology, Writing – original draft, Data curation. **F. Batalioto:** Conceptualization. **A.M. Figueiredo Neto:** Conceptualization. **I. Lelidis:** Conceptualization, Methodology, Writing – original draft, Formal analysis, Data curation, Writing – review & editing, Visualization.

Acknowledgement

G.B. acknowledges partial support by Moscow Engineering Physical Institute (MEPhI). F.B. and A.F.N acknowledge partial support by INCT/CNPq (Conselho Nacional de Desenvolvimento Científico e Tecnológico; Grant Number: 465259/2014-6), INCT/FAPESP (Fundação de Amparo à Pesquisa do Estado de São Paulo; Grant Number: 14/50983-3), INCT/CAPES (Coordenação de Aperfeiçoamento de Pessoal de Nível Superior; Grant Number: 88887.136373/2017-00), FAPESP (Thematic Project; Grant 2016/24531-3), and INCT-FCx (Instituto Nacional de Ciência e Tecnologia de Fluidos Complexos).

References

[1] E. Barsoukov, J.R. Macdonald, Impedance spectroscopy: Theory, experiment, and applications, Impedance Spectroscopy: Theory, Experiment, and Applications, 2nd, John Wiley & Sons, New Jersey, 2005.
[2] J.R. Macdonald, Theory of ac Space-Charge Polarization Effects in Photoconductors, Semiconductors, and Electrolytes, Phys. Rev. 92 (1953) 4, doi:10.1103/PhysRev.92.4.
[3] D.R. Franceschetti, Small-signal ac response of supported thin-layer electrochemical cells, J. Chem. Phys. 86 (1987) 6495, doi:10.1063/1.452440.
[4] J. Jamnik, J. Maier, Treatment of the Impedance of Mixed Conductors Equivalent Circuit Model and Explicit Approximate Solutions, J. Electrochem. Soc. 146 (1989) 4183, doi:10.1149/1.1392611.
[5] J. Bisquert, Theory of the Impedance of Electron Diffusion and Recombination in a Thin Layer, J. Phys. Chem. B 106 (2002) 325, doi:10.1021/jp011941g.
[6] K.J. Klein, S. Zhang, S. Dou, B.H. Jones, R.H. Colby, R. Runt, Modeling electrode polarization in dielectric spectroscopy: Ion mobility and mobile ion concentration of single-ion polymer electrolytes, J. Chem. Phys. 124 (2006) 144903, doi:10.1063/1.2186638.
[7] G. Barbero, A.L. Alexe-Ionescu, Role of the diffuse layer of the ionic charge on the impedance spectroscopy of a cell of liquid, Liq. Cryst. 32 (2005) 943, doi:10.1080/02678290500228105.
[8] G. Derfel, Numerical study of ionic current in dielectric liquid layer subjected to ac voltage, J. Mol. Liq. 144 (2009) 59, doi:10.1016/j.molliq.2008.10.007.
[9] Y. Wang, C.N. Sun, F. Fan, J.R. Sangoro, M.B. Berman, S.G. Greenbaum, T.A. Zawodzinski, A.P. Sokolov, Examination of methods to determine free-ion diffusivity and number density from analysis of electrode polarization, Phys. Rev. E 87 (2013) 042308, doi:10.1103/PhysRevE.87.042308.
[10] A. Serghei, M. Tress, J.R. Sangoro, F. Kremer, Electrode polarization and charge transport at solid interfaces, Phys. Rev. B 80 (2009) 184301, doi:10.1103/PhysRevB.80.184301.
[11] M. Samet, V. Levchenko, G. Boiteux, G. Seytre, A. Kaiei, A. Serghei, Electrode polarization vs. Maxwell-Wagner-Sillars interfacial polarization in dielectric spectra of materials: Characteristic frequencies and scaling laws, J. Phys. Chem. 42 (2015) 194703, doi:10.1063/1.4919877.
[12] A. Santoro, J.L. de Paula, E.K. Lenzi, L.R. Evangelista, Anomalous diffusion governed by a fractional diffusion equation and the electrical response of an electrolytic cell, J. Chem. Phys. 135 (2011) 114704, doi:10.1063/1.3637944.
[13] L. Landau, E. Lifchitz, Physique théorique: Electrodynamique des milieux continus, MIR, Moscou, 1990.
[14] G. Barbero, A.L. Alexe-Ionescu, I. Lelidis, Significance of small voltage in impedance spectroscopy measurements on electrolytic cells, J. Appl. Phys. 98 (2005) 113703, doi:10.1063/1.2137444.
[15] P.W. Atkins, Physical chemistry, 5th, Oxford University Press, Oxford, 1994.
[16] G. Barbero, M.J. Scalerandi, Similarities and differences among the models proposed for real electrodes in the Poisson-Nernst-Planck theory, J. Chem. Phys. 136 (2012) 084705, doi:10.1063/1.3686767.
[17] R.L.V. Meirhaeghe, E.C. Dutoit, F. Cardon, W.P. Gomes, On the application of the Kramers-Kronig relations to problems concerning the frequency dependence of electrode impedance, Electrochim. Acta 20 (1975) 995–999, doi:10.1016/0013-4686(75)85062-6.

[18] A. Weiß, S. Schindler, S. Galbiati, M.A. Danzer, R. Zeis, Distribution of Relaxation Times Analysis of High-Temperature PEM Fuel Cell Impedance Spectra, Electrochim. Acta 230 (2017) 391–398, doi:10.1016/j.electacta.2017.02.011.
[19] J.J. Giner-Sanz, E.M. Ortega, V. Perez-Herranz, Application of a Montecarlo based quantitative Kramers-Kronig test for linearity assessment of EIS measurements, Electrochim. Acta 209 (2016) 254–268, doi:10.1016/j.electacta.2016.04.131.
[20] F. Batalioto, G. Barbero, A.F.C. Campos, A.M.F. Neto, Free ions in kerosene-based ferrofluid detected by impedance spectroscopy, Phys. Chem. Chem. Phys. 23 (2021) 2819, doi:10.1039/D0CP05865C.
[21] A.L. Alexe-Ionescu, G. Barbero, I. Lelidis, Complex Dielectric Constant of a Nematic Liquid Crystal Containing Two Types of Ions: Limit of Validity of the Superposition Principle, J. Phys. Chem. B 113 (2009) 14747–14753, doi:10.1021/jp906479w.
[22] I. Lelidis, G. Barbero, A. Sfarna, Comparison of two generation-recombination terms in the Poisson-Nernst-Planck model, J. Chem. Phys. 137 (2012) 154104, doi:10.1063/1.4757020.
[23] A.M. Antonova, G. Barbero, F. Batalioto, A.M.F. Neto, K. Parekh, Electric response of cells containing ferrofluid particles, J. Electroanal. Chem. 856 (2020) 113479, doi:10.1016/j.jelechem.2019.113479.
[24] M.E. Trukhan, Dispersion of the dielectric constant of heterogeneous systems, Sov. Solid State 24 (1963) 2560.
[25] J.L. de Paula, P.A. Santoro, R.S. Zola, E.K. Lenzi, L.R. Evangeista, F. Ciuchi, A. Mazzulla, N. Scaramuzza, Non-Debye relaxation in the dielectric response of nematic liquid crystals: Surface and memory effects in the adsorption-desorption process of ionic impurities, Phys. Rev. E 86 (2012) 051705, doi:10.1103/PhysRevE.86.051705.
[26] F. Ciuchi, A. Mazzulla, N. Scaramuzza, E.K. Lenzi, L.R. Evangelista, Fractional Diffusion Equation and the Electrical Impedance: Experimental Evidence in Liquid-Crystalline Cells, J. Phys. Chem. C 116 (2012) 8773, doi:10.1021/jp211097m.
[27] A.L. Alexe-Ionescu, G. Barbero, S. Bianco, G. Cicero, C.F. Pirri, Electrical response of electrolytic cells limited by different types of electrodes, J. Electroanal. Chem. 669 (2012) 21–27, doi:10.1016/j.jelechem.2012.01.015.
[28] I. Lelidis, J.R. Macdonald, G. Barbero, Poisson-Nernst-Planck model with Chang-Jaffe, diffusion, and ohmic boundary conditions, J. Phys. D: Appl. Phys. 49 (2015) 025503, doi:10.1088/0022-3727/49/2/025503.
[29] M.E. Orazem, B. Tribollet, Electrochemical impedance spectroscopy, John Wiley, Hobocken, 2008.
[30] T.J.V.d. Noot, Hilbert transformation of immittance data using the Fast Fourier Transform, J. Electroanal. Chem. 322 (1992) 9–24, doi:10.1016/0022-0728(92)80064-B.
[31] B.A. Boukamp, Practical application of the Kramers-Kronig transformation on impedance measurements in solid state electrochemistry, Solid State Ion. 62 (1993) 131–141, doi:10.1016/0167-2738(93)90261-Z.
[32] B.A. Boukamp, A Linear Kronig-Kramers Transform Test for Immittance Data Validation, J. Electrochem. Soc. 142 (1995) 1885–1894, doi:10.1149/1.2044210.
[33] S. Cruz-Manzo, R. Chen, A generic electrical circuit for performance analysis of the fuel cell cathode catalyst layer through electrochemical impedance spectroscopy, J. Electroanal. Chem. 694 (2013) 45–55, doi:10.1016/j.jelechem.2013.01.037.
[34] I. Lelidis, G. Barbero, Negative Capacitance of an Electrolytic Cell in the Absence of Bias Potential, J. Phys. Chem. C 118 (2014) 8245–8252, doi:10.1021/jp412095h.